Eur. Phys. J. Spec. Top.
https://doi.org/10.1140/epjs/s11734-024-01296-y

THE EUROPEAN PHYSICAL JOURNAL SPECIAL TOPICS

Regular Article

Influence of dimethyl sulfoxide on membrane fluidity under rapid supercooling

Samapika Sahu, Prasanjit Dutta, and Ananya Debnath[a]

Department of Chemistry, Indian Institute of Technology, Jodhpur, Jodhpur, Rajasthan 342030, India

Received 4 April 2024 / Accepted 2 August 2024

Abstract The effect of dimethyl sulfoxide (DMSO) on a model 1,2-dimyristoyl-sn-glycero-3-phosphocholine lipid membrane is investigated during a rapid supercooling from 350 to 250 K using a total of 165.0198 μs all-atom molecular dynamics simulations. Our findings reveal that the addition of DMSO above a critical concentration induces significant alterations in the gel phase of the membrane at supercooled temperatures, shifting the gel phase to a fluid phase evident from area per lipid, order parameter, and d-spacing. Notably, an anomalous contraction is observed in bilayers in the presence of DMSO with the same critical concentrations as the temperature is cooled from 300 K. As the concentration of DMSO rises at supercooled temperatures, the interface becomes increasingly populated with DMSO molecules, approaching a two-dimensional percolation threshold. This process leads to an expansion in the area occupied by each lipid molecule, creating free space around the lipid tails. Subsequently, the population of DMSO and water at the hydrophobic core becomes energetically favorable at a supercooled temperature compared to the higher temperature above the critical concentration of DMSO. The higher population of DMSO and water at the interface and at the hydrophobic core increases the disorder and fluidity of the lipids and gradually changes the gel phase toward the fluid phase. Thus, our results provide the molecular mechanism of DMSO-induced fluidity of the membrane at supercooled temperature relevant for cell banking in the future.

1 Introduction

Membranes comprising lipid molecules act as a semipermeable barrier to the cell and serve as a matrix to many cellular components such as protein, carbohydrate, sugar, and so on. Membranes regulate many cellular functions like permeability, transport, and signal transduction. The cell membranes remain active in their fluid phase as they allow the motion of molecules needed for their functions. At supercooled temperature, the molecular motions are dramatically reduced, leading to frozen biochemical reactions, and the membranes undergo a fluid-to-gel phase transition, which makes the membrane functionally inactive. When exposed to extremely low temperatures, cell membranes experience mechanical and physical stresses, such as ice crystallization and growth, increased salt content, and cell dehydration. This has the potential to alter the functional behavior of the membranes or cause the membranes to cease functioning, leading to apoptosis, thus rendering the cells useless for transplant [1, 2]. Thus, keeping the cell membranes functionally active at supercooled temperature is pivotal for prolonged storage of the live cells needed for cryopreservation [3] with applications such as organ transplantation, in vitro fertilization, cell and tissue culture, and drug development [4]. To achieve vitrification, high concentrations of both permeating and non-permeating CPAs are needed such as ethylene glycol, propylene glycol, sugars, DMSO, and macromolecular compounds such as poly(vinyl alcohol) co-poly(vinyl acetate) (PVA-co-PVAc) copolymers and carboxylated ϵ-poly-L -lysine(COOH-ϵ PLL), serum protein, dextran, PEG, and hydroxyethyl starch [5–7].

The addition of DMSO has been a popular approach to overcome the challenges due to rapid cooling during cryopreservation [3, 8]. DMSO is a well-known co-solvent largely used in chemistry and biology and frequently used in cell banking. It is the most popular cell membrane permeating cryoprotective agent (CPA) with low cost and low toxicity. Due to its compatible size and stable structure, it can easily enter the membrane and does not react with the interior environment. There is an appearance of short-lived transient pores where DMSO and

[a] e-mail: ananya@iitj.ac.in (corresponding author)

Published online: 22 August 2024

water molecules penetrate the bilayer at 350 K [9]. The increased concentration of DMSO induces disorder in the bilayer at 350 K without disintegrating the bilayer. Other guest molecules such as drugs enhance the lipid dynamics and induce more order to the cationic bilayer [10]. Ethanol as a disinfectant and hand sanitizer can induce swelling, rupturing, aggregation, and fusion of lipid vesicles in a concentration-dependent manner [11]. DMSO can modulate the properties of cell membranes by altering the solvent properties and increasing the solution viscosity at supercooled temperatures [12]. DMSO is typically added to the media used for freezing cells at a concentration ranging from 5 to 15% to protect them from harsh conditions [13, 14]. When added to media, DMSO prevents intracellular and extracellular ice crystal formation during freezing. However, when DMSO is added at a higher concentration than 25%, cell lysis happens due to increased toxicity [15]. Therefore, a comprehensive understanding of the DMSO-induced phase behavior of membranes is essential to mitigate the challenges during cryopreservation.

Rapid cooling during vitrification is a clinically used method for cryopreservation of embryos where a higher concentration of DMSO is applied [16]. This leads to the formation of an amorphous glassy state below glass transition temperature by avoiding heterogeneous or homogeneous ice nucleation. As a higher concentration of DMSO can induce toxicity, the CPA should be removed rapidly in a stepwise fashion to avoid post-thaw toxicity and damage due to osmotic stress. Apart from these, DMSO has demonstrated its capability to induce epigenetic modifications in hepatic microtissues [17], promote differentiation in embryonic stem cells [18], and contribute to the leaching of plasticizers from cell storage bags [19]. Moreover, while DMSO can elicit adverse effects in patients who receive cryopreserved transplanted material, it is important to acknowledge that the clinical benefits of the transplant outweigh these concerns [20, 21].

Previous studies on various bilayers with varying concentrations of DMSO using simulations suggest that DMSO selectively penetrates much deeper into the bilayer than water due to its amphiphilic nature, dehydrating the headgroups [22, 23]. At physiological temperature, DMSO with different kinds of membranes has been extensively studied and DMSO is known to induce fluidity to the bilayer, increase the area per lipid, reduce the bilayer thickness, and form transient pores [24–26]. These amphiphilic molecules render softer membranes [27–30]. Poration-free energy calculated in our previous work suggests that with an increase in DMSO concentration, the energy barrier of DMSO crossing is lowered only when it is facilitated by the water [9]. The role of hydrogen bonding is explored for three major regimes from low to fully hydrated bilayers, which modulates the molecular mechanisms [31]. Experimentally, it has been found that the effect of DMSO on lipid bilayers is dependent on the lipid type [23].

In this study, the effect of varying concentrations of DMSO is investigated on model DMPC membranes across temperatures ranging from much above the bilayer melting to a supercooled regime. The insertion of different concentrations of DMSO into the bilayer at supercooled temperatures alters the gel phase of the bilayer to a fluid phase, evident from different structural properties such as area per lipid head, order parameter, and d-spacing. The drastic change in the area per lipid head is associated with a slow shift of fractal dimension of the continuously residing interfacial DMSO toward the percolation threshold, suggesting the significant contribution of interfacial DMSO in the gel-to-fluid phase transition. Our analyses provide the molecular mechanism of the DMSO-induced bilayer phase transition at supercooled temperature. The results can be extended and applicable for plasma membranes under cold stress in the future.

2 Simulation details and methods

In this study, all-atom molecular dynamics (MD) simulations are performed starting from a pre-equilibrated DMPC lipid bilayer at 350 K [9] consisting of 128 lipids in the presence of 5744 water molecules. Slipid force field is used for lipids [32, 33], and TIP4P/2005 is used for water [34]. The DMSO parameters are derived from general Amber force field (GAFF) [35, 36]. DMSO is used as a co-solvent in the bilayer with concentrations varying from 0 to 25% as shown in Table 1. The structures of DMPC and DMSO are shown in Fig. 1. The supercooled regime is achieved by simulation annealing each bilayer containing 0% to 25% DMSO at 350 K to 250 K at 10 K interval with an annealing rate of 1 K/ns. The annealing rate in our study is one order of magnitude slower than that for other cryoprotective agents reported earlier [8] and many orders of magnitudes faster than the rate used in cryopreservation techniques [37]. Thus, the rate of cooling in our study is considered to be a rapid cooling relevant for vitrification. A total number of 66 bilayers are simulated with 6 different DMSO concentrations and 11 different temperatures. The simulation run lengths for all bilayers at each concentration are presented in Table 1. The box dimension details of all simulated bilayers are provided in Table S1 of the supplementary information (SI).

The Lennard–Jones interactions are shortened using a dual range cutoff of a distance of 1 nm and 1.4 nm. The pair-step is thereafter modified after every sequence of ten steps. Particle-mesh Ewald (PME) technique is used for electrostatic interactions [38]. The equilibration simulations are conducted using the NPT ensemble with semi-isotropic pressure coupling. The temperature and pressure are regulated with the Berendsen thermostat [39] and barostat [40] with a coupling constant of 2 ps. Subsequently, production NPT runs involve velocity-rescale thermostat [41] and Parrinello–Rahman barostat [42] at 1 bar using parameters consistent with those of

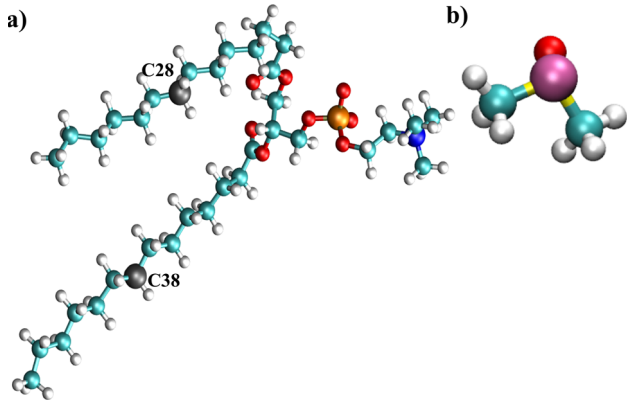

Fig. 1 Structure of **a** DMPC lipid, carbon atoms C28 and C38 are highlighted and **b** DMSO molecule. Color code: carbon: cyan; phosphorus: orange; nitrogen: blue; oxygen: red; hydrogen: white; sulfur: pink

Table 1 Details of bilayers and a total of 165.0198 μs simulation runs

Number of bilayers for each concentration	Percentage of DMSO	Total equilibration runlength (ns)	Total production runlength (ns)
11	0%	11 × 2000 = 22,000	500.3 × 11 = 5503.3
11	5%	11 × 2000 = 22,000	500.3 × 11 = 5503.3
11	10%	11 × 2000 = 22,000	500.3 × 11 = 5503.3
11	15%	11 × 2000 = 22,000	500.3 × 11 = 5503.3
11	20%	11 × 2000 = 22,000	500.3 × 11 = 5503.3
11	25%	11 × 2000 = 22,000	500.3 × 11 = 5503.3

Each DMSO concentration constitutes 11 sets of bilayers for temperatures ranging from 250 to 350 K. Each bilayer has been equilibrated for 2 μs and the production simulation for each bilayer is 500.3 ns

equilibration runs. The integration time step of 2 fs is consistently applied for each simulation. Simulations are performed with GROMACS version 2020.2 [43].

The area per lipid head (APLH, A_{h}) of the bilayers are calculated by

$$A_{\mathrm{h}} = \frac{b_x \times b_y}{N_{\mathrm{l}}}, \tag{1}$$

where b_x and b_y are simulation box lengths along the x and y axes of the bilayer surface and N_{l} denotes the total number of lipids in each leaflet.

Order parameter is calculated by

$$S_{\mathrm{CH}} = \frac{1}{2}\langle 3cos^2\theta - 1\rangle, \tag{2}$$

where θ is the alignment angle subtended by the alkyl chains with respect to the bilayer normal (z-direction). $\langle\rangle$ corresponds to the ensemble and time averaging.

The potential of mean force (PMF) is calculated by taking the Boltzmann inversion of the respective density (ρ) with respect to their bulk density (ρ_0) along the bilayer normal using the following equation:

$$\mathrm{PMF} = -k_{\mathrm{BT}} ln\frac{\rho}{\rho_0}. \tag{3}$$

The last 250 ns of a 500 ns NPT production run with a saving frequency of 50 ps is utilized to analyze the bilayer structural properties such as area per lipid, order parameter, density profile, d-spacing, and PMF. Further, the last 250 ps of a 300 ps NVT trajectory with a saving frequency of 0.1 ps is divided into five blocks of 50 ps and is used to calculate the population of the continuously residing DMSO and water in the interfacial and hydrophobic layers of all the bilayers. The cumulative radial distribution function and mean square displacement are calculated from the last 50 ps of the 300 ps NVT production analysis with a saving frequency of 0.1 ps to determine the percolation threshold.

3 Results and discussion

The snapshots of the final configurations of bilayers with 0% and 25% DMSO concentrations are shown for all temperatures in Fig. 2. The snapshots of the remaining bilayers with 5–20 % DMSO are shown in Figure S1 of SI.

3.1 Area per lipid head

The APLH, A_h, is a crucial parameter that can monitor the phase behavior of lipid bilayers. The equilibration of each bilayer is confirmed from the converged APLH (shown in Figure S2 of SI). The APLH of each bilayer is averaged over time and plotted with respect to temperature for all DMSO concentrations in Fig. 3a. The APLHs of bilayers in the absence of DMSO using Slipid force field as in the current study is shown by the black solid line in Fig. 3a. The APLH decreases with cooling and has a sharp transition below 300 K, indicating a fluid-to-gel phase transition. The phase transition temperature and the behavior of APLH with respect to temperature from our current study are in reasonable agreement with that from the CHARMM force field (shown by a black dashed line) from our previous work [44] and other available literature [45–47] (compiled and shown in dark blue). This confirms that the Slipid force field can capture the phase transition of the DMPC bilayer in the absence of DMSO reasonably well. Note that the ripple phase of DMPC is not well captured using the Slipid force field as obtained using CHARMM force field [44, 48–53].

With the addition of DMSO in the bilayer, the APLH increases for all temperatures. When the temperature is cooled from 350 K to 250 K, the APLH decreases with temperature until a DMSO critical concentration of 15%. For DMSO concentrations of 20% and 25%, the APLH at 350 K is maximum, then with cooling, it lowers down to a value of 0.67 nm^2 and then subsequently increases to a value of 0.75 nm^2. Both experimental and computational findings [44, 45] suggest that at an APLH value of nearly 0.60 nm^2, the bilayer attains a fluid phase. Thus, the addition of 15% DMSO slowly shifts the supercooled bilayer from the gel to the fluid phase. For bilayers with 20% and 25% DMSO, the APLH decreases with cooling till 300 K and then increases to 250 K. The comparable values of APLH for 250 and 350 K indicate that the bilayers are at the fluid phase at supercooled temperature when the DMSO concentrations are 20 and 25%.

3.1.1 Order parameter

The order parameter of lipid acyl chains refers to a measure of the degree of alignment of the acyl chains of lipid molecules with respect to the bilayer normal. The order parameter increases with supercooling until 15% DMSO concentration in the bilayer as shown in Fig. 3b. This signifies the chains in the bilayer become more ordered with supercooling until a critical concentration of DMSO. However, the addition of DMSO significantly reduces the order parameter at supercooled temperature, demonstrating that the chains become more disordered. For 20% and 25% concentrations of DMSO, the order parameter of the bilayer increases to 300 K and then reduces till supercooled temperature. The similar values of the order parameter of the bilayers at 250 K and 350 K with 20% and 25% DMSO indicate that the bilayer attains a similar disorder of a fluid phase at the supercooled temperature.

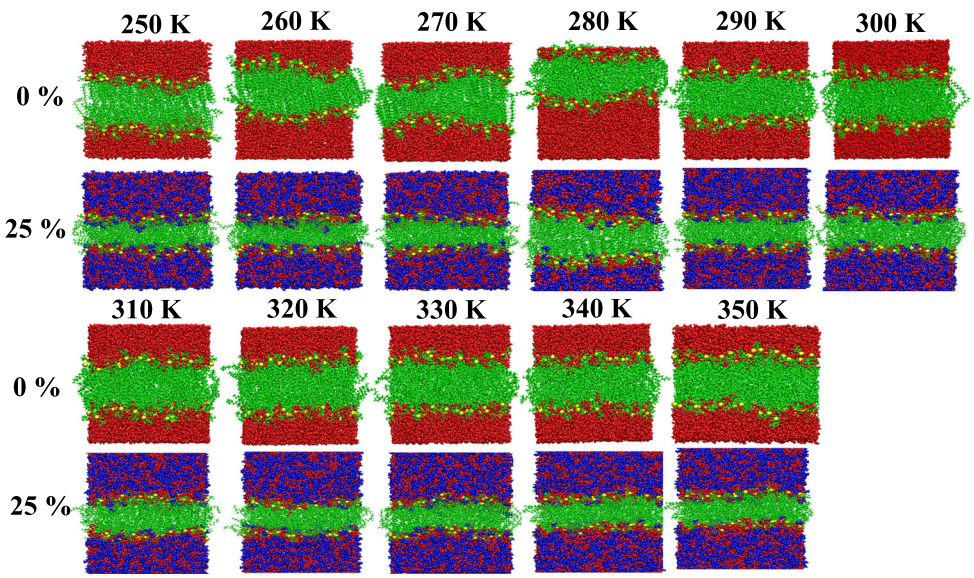

Fig. 2 Bilayer snapshots for all studied temperatures for the DMSO concentrations of 0% and 25%. Color code: water: VDW, red; phosphorus: yellow, VDW; lipids: green, licorice; DMSO: blue, VDW

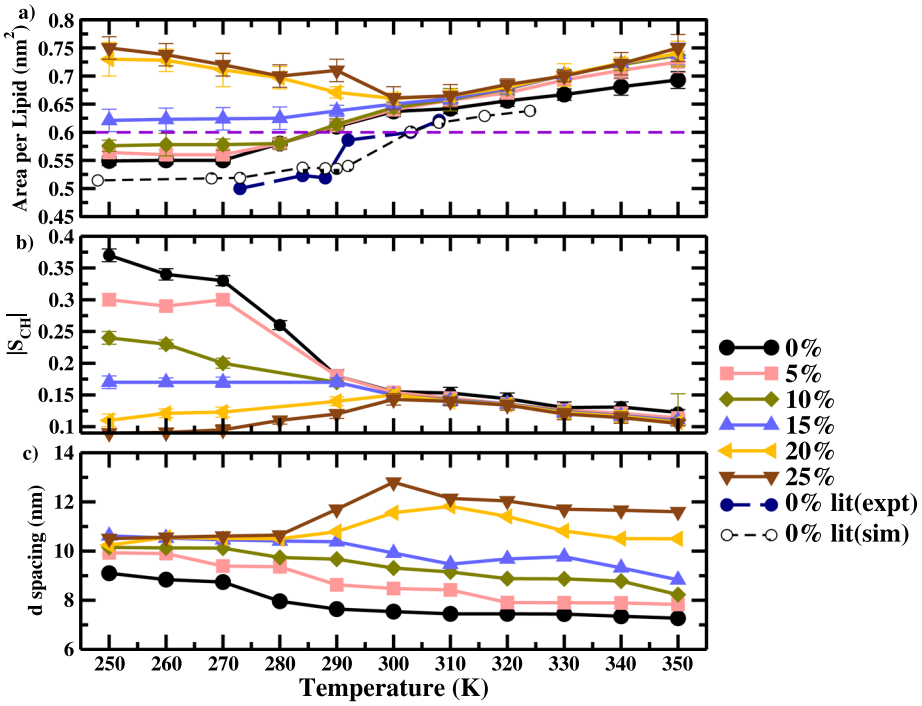

Fig. 3 **a** Area per lipid head of bilayers across the temperature ranges from 350 to 250 K. The APLH values of the bilayer without DMSO from our simulations using Slipid force field are compared with the ones using CHARMM force field [44, 48, 49, 54] and experimental findings [45–47]. The dashed violet line represents the APLH cutoff above which the bilayer is considered at the fluid phase. **b** Average order parameter of alkyl chains and **c** d-spacing of bilayers comprising 0% to 25% of DMSO across all temperatures

This indicates that the bilayers slowly shift from the gel phase to the fluid phase at a supercooled temperature in the presence of 20–25% DMSO concentration. Note that the order parameters of the chains of these two bilayers start reducing from 300 K when their APLH starts increasing.

3.1.2 d-Spacing

The d-spacing of the bilayer is determined by time averaging of the box length along the z-direction, which is the direction of the bilayer normal. As the bilayers become more fluid, the d-spacing reduces substantially. For DMSO concentrations from 0 to 15%, the d-spacing increases with supercooling. For bilayers with 20 and 25%, the d-spacing drastically decreases from 300 K to 280 K as shown in Fig. 3c. This deviation from normalcy is attributed to an anomalous contraction of the bilayer as the bilayer is cooled from 300 to 280 K. Similar anomalous contraction (referred to as anomalous swelling in case of heating) is reported earlier for the surfactant, co-surfactant bilayers without DMSO [55]. During the anomalous swelling from supercooled to higher temperatures within 280–300 K, there is an elongation of lipid chains, hence inducing more order in the chains, which reduces APLH as well. The lower d-spacing of the bilayers with 20% and 25% DMSO at 250 K than at 350 K in association with higher APLH and lower-order parameter suggests that the bilayer is in the fluid phase at supercooled temperature above a critical concentration of DMSO.

3.1.3 Density profile

Density profiles of lipid, water, and DMSO are shown for all cases in Figures S3 and S4 of SI. With an increase in DMSO concentration, the density of water decreases, and the density of DMSO increases for all temperatures. A comparison of the density profiles of the bilayer at two extreme temperatures, supercooled temperature, 250 K, and higher temperature, 350 K, shows that both DMSO and water penetrate in the hydrophobic region to a larger extent at 250 K compared to that at 350 K for 20 and 25% DMSO (Fig. 4). Since the d-spacings of the bilayer with 20 and 25% DMSO are smaller at 250 K compared to that at 350 K and more water and DMSO penetrate in the hydrophobic core with supercooling (Fig. 3c), these water and DMSO in the hydrophobic core are responsible for the fluidity of the lipid chains. The longer d-spacing of the bilayer at 350 K compared to that at 250 K is consistent with the elongation of the density profile along the bilayer normal.

Our earlier investigation shows that the interfacial DMSO not only settles near the interface, but penetrates into the hydrophobic core by acquiring the thermal energy from the fluctuations of the disordered interface and reshuffling of some water molecules from the interface to the bulk and eventually crosses the hydrophobic barriers with the aid of water [9]. This mechanism should prevail for the bilayer at a supercooled temperature at 250 K in the presence of 20% and 25% DMSO. As shown in Figure S4 of SI, more DMSO and water for the bilayer with

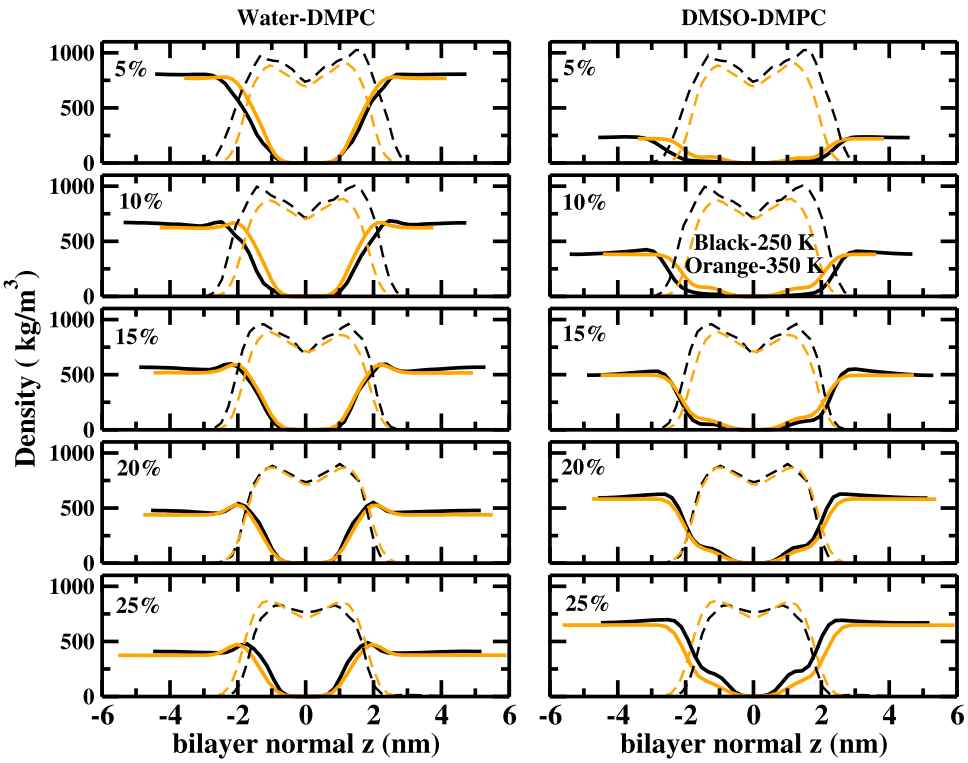

Fig. 4 Density profile for water, DMSO, and lipids shown for all DMSO concentrations with two extreme temperatures, 250 K and 350 K. Color code: black: 250 K, orange: 350 K. Solid lines refer to water density for the left panel and DMSO density for the right panel. Dashed lines refer to the density profile of DMPC lipids for all panels

25% DMSO reside at the bulk regime at 350 K, whereas at 250 K, they reside in the hydrophobic core. Thus, at elevated temperatures, there is a high probability of DMSO and water migration toward bulk, and at supercooled temperatures, the probability of migration toward the hydrophobic core increases. The increased density of DMSO and water in the hydrophobic core increases the disorder of the chains at supercooled temperature. Thus, a higher concentration of DMSO increases the fluidity of the bilayer at supercooled temperature.

The bulk (B), interface (I), and hydrophobic core (HC) are identified from the density profiles of water, DMPC lipids, and DMSO. The difference in the PMF between the bulk as the final state and the interface as the initial state is considered the free energy difference between the interface to the bulk (ΔG_{I-B}). Similarly, the difference in the PMF between the hydrophobic core as the final state and the interface as the initial state is considered as the free energy difference between the interface to the hydrophobic core ($\Delta G_{I-\mathrm{HC}}$). Thus, ΔG_{I-B} and $\Delta G_{I-\mathrm{HC}}$ provide estimates of free energy costs for the interface water or DMSO to move to the bulk and to the hydrophobic core, respectively. The free energy difference for DMSO and water molecules from the interface to the bulk (B) and to the hydrophobic core are studied for two extreme temperatures as shown in Fig. 5. The negative ΔG_{I-B} implies that the bulk is favorable compared to the interface and the positive $\Delta G_{I-\mathrm{HC}}$ signifies that the interface is always favorable compared to the hydrophobic core for all cases. The energy cost for DMSO to migrate from the interface to the bulk increases with an increase in DMSO concentrations for both temperatures. However, at 250 K, ΔG_{I-B} increases above 15%, suggesting that the interface DMSO needs higher energy to go to the bulk state at supercooled temperature compared to that at 350 K. In contrast, ΔG_{I-B} of water decreases with DMSO concentration at 250 K. Thus, less energy cost is needed for water to move from the interface toward the bulk with increasing DMSO concentrations at 250 K. At 350 K, with increasing DMSO concentration, DMSO and water are more tightly bound at the interface. Hence, DMSO or water migration toward bulk requires more energy with increasing DMSO concentration at 350 K. Therefore, the probability of water migrating from the interface to the bulk is higher at supercooled temperature compared to that at 350 K with increasing concentration of DMSO. This suggests that the probability of water replacement and dehydration by DMSO at the interface is more at 250 K with increasing concentration of DMSO. In contrast, water residence at the interface is assisted with DMSO at 350 K with increasing concentration of DMSO. The opposing effect of water association with DMSO at 350 K and water replacement by DMSO at 250 K results in contrasting behavior of water at two extreme temperatures. Notably, the $\Delta G_{I-\mathrm{HC}}$ of DMSO decreases with an increase in the concentration of DMSO at both extreme temperatures. A similar trend prevails for water except at 25% (Fig. 5c, d). At 25%, DMSO and water entering the HC become more favorable at 250 K compared to that at 350 K. The lowering in $\Delta G_{I-\mathrm{HC}}$ of the DMSO and water at 25% DMSO concentration and at supercooled temperature suggests that both the DMSO and water residing in the HC become favorable with increasing concentration of DMSO with supercooling which can lead to the DMSO-induced disorder or fluidity of the lipid chains at the supercooled temperature.

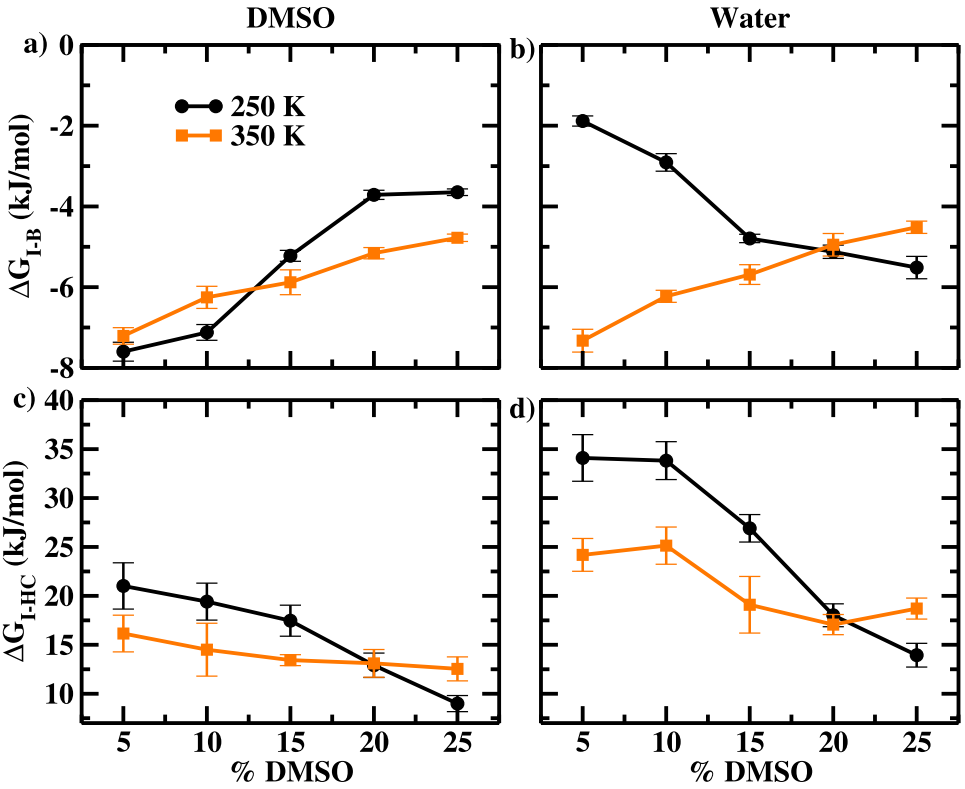

Fig. 5 Free energy difference calculated between (**a**, **b**) the interface (I) and bulk (B) for DMSO and water, respectively, and **c**, **d** the interface (I) to hydrophobic core (HC) for bilayers at 250 K and 350 K containing different DMSO concentrations. The error bar depicts the average over five sets of data

3.1.4 Definition of water and DMSO at the interface and hydrophobic core

The first coordination shell of water and DMSO for the lipid heads (phosphorus) is at ~ 0.55 nm [9]. Thus, the interfacial region of each bilayer is chosen as the 0.55 nm above and below the lipid head atoms (Fig. 6). The DMSO and water molecules that continuously reside within ± 0.55 nm of the lipid heads for 50 ps are labeled as interfacial water (IW) and interfacial DMSO (ID). These specific water and DMSO are considered bound to the interface. Our earlier results show that the residence time of IW is 100 ps. However, 50 ps is considered the residence time as it gives reasonable statistics to both the numbers of IW and ID for all cases.

The hydrophobic core (HC) refers to the region situated between the upper and lower interfacial regions of the bilayer. The first peak of the $g(r)$ of lipid P head and the lipid tail bead, C28 or C38, is located at > 1.25 nm

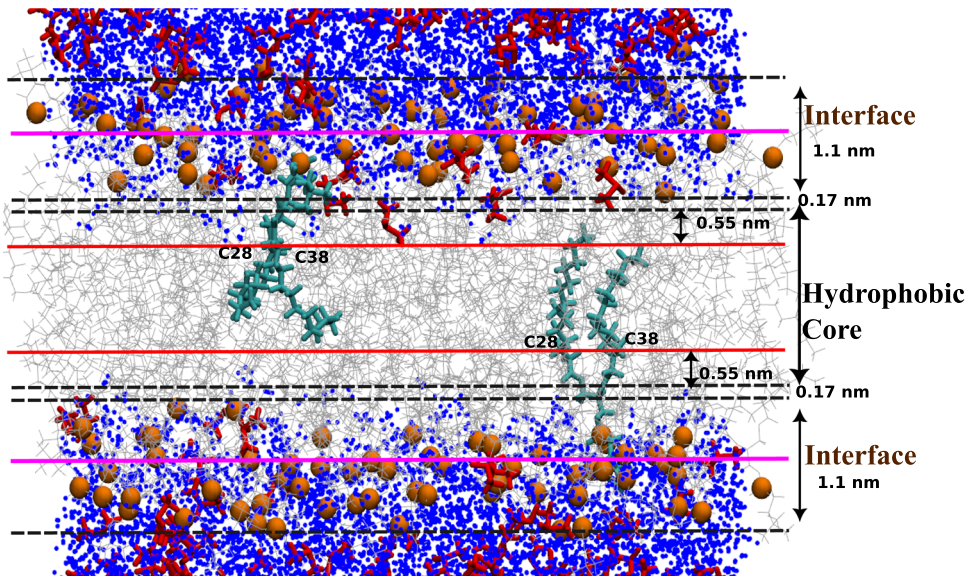

Fig. 6 Snapshot of a bilayer containing 5% DMSO concentration at 350 K, representing the regions defined as the interface and hydrophobic core. The magenta and red solid lines denote the average location of the head (P-atom) and the carbon atoms C28 and C38 of lipids. Color code: water: points, blue; phosphorus: orange, VDW; lipids: gray, lines; DMSO: red, QuickSurf. Two lipids are highlighted (licorice, cyan) from the upper and lower leaflet to denote the average positions of C28 and C38 of the two tails

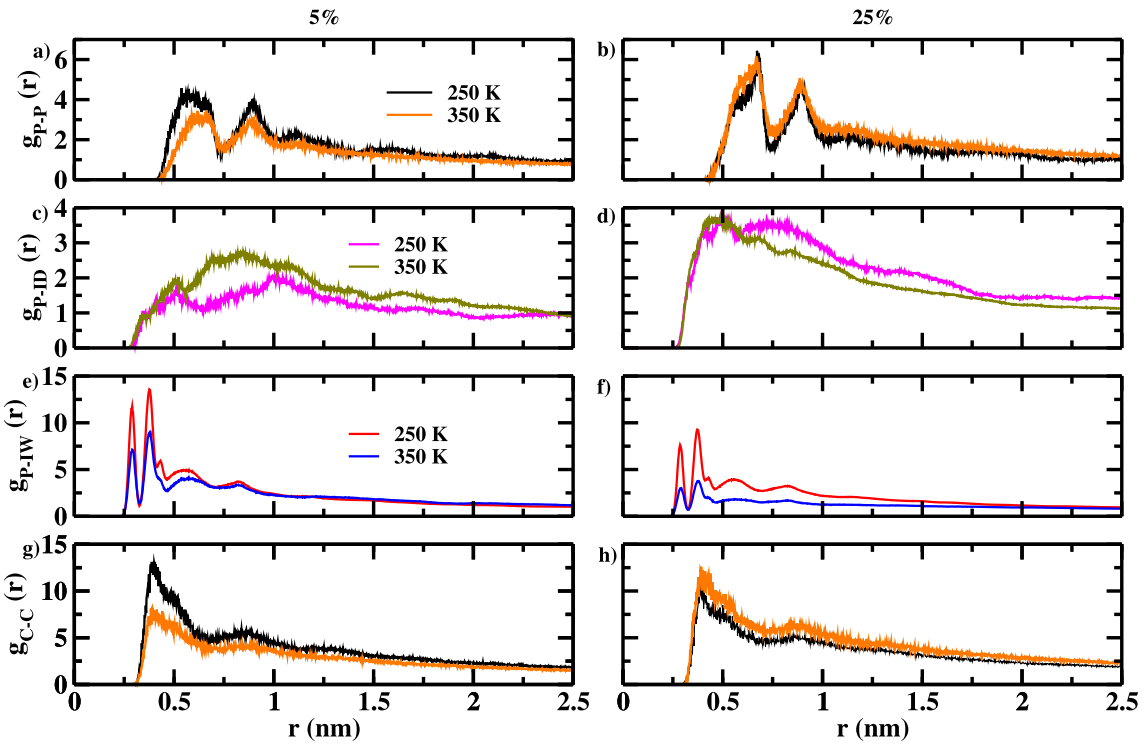

Fig. 7 Comparison of the radial distribution function, $g(r)$ of **a**, **b** lipid P–P (phosphorus) head; **c**, **d** P–ID (phosphorus–interfacial DMSO); **e**, **f** P–IW (phosphorus–interfacial water); **g**, **h** lipid C–C (end carbon atoms of lipid tails) for the supercooled 250 K and 350 K for 5% and 25% DMSO. Data from other concentrations and temperatures are omitted for clarity. The $g(r)$ reaches a value of 1 at larger r

(as shown in Figure S6 of SI). The C28 or C38 atoms of the lipid tails from both the lower and the upper leaflets are considered the periphery of the HC (Fig. 6). Any DMSO and water molecules that fall within a distance of 0.55 nm from the lipid tail beads residing within the hydrophobic region for at least one time frame throughout the 50 ps simulation period are considered as the water and DMSO in the HC. To get reasonable statistics on the number of DMSOs and water in the HC, the continuously residing molecules are avoided. The geometric criteria ensure that there is no overlap between the interface regime and the HC as seen in Fig. 6.

3.2 Radial distribution function

The three-dimensional radial distribution function, $g(r)$, quantifies the radial association of neighboring molecules around each other and is calculated by the following equation:

$$g(r) =< \frac{1}{\rho_N} \sum_{i=1}^{N} \sum_{j=1}^{N} \delta(r_{ij} - r) >, \tag{4}$$

where N denotes the total number of molecules and ρ_N the density of the molecules. Figure S5 of SI shows that $g(r)$ of lipid heads and tails of the bilayers attain higher order in the absence of DMSO as one approaches supercooling from 350 K. As the bilayer with 0%, DMSO is in the fluid phase at 350 K, which changes to a gel phase at 250 K, and the order of both the head and tails of the lipids increases with supercooling. With the addition of 5% DMSO, a similar trend prevails (Fig. 7a, b). With an increase in DMSO concentration, the behaviors slowly change, and at 25% DMSO concentration, the behavior is the opposite. At supercooled temperature, both the lipid heads and tails with 25% DMSO have comparable or are less structured than that at 350 K, indicating similar disorder in the bilayers at these two temperatures. This again suggests that the bilayer slowly shifts from a gel-to-fluid phase at supercooled temperature due to the addition of DMSO.

The $g(r)$ of the lipid head and the IW and ID in Fig. 7 depict that both the IW and ID intercalate between the lipid heads for all cases. IW becomes more ordered due to supercooling. As DMSO concentration increases from 5 to 25%, the amplitudes of $g(r)$ of the IW decrease for all temperatures, which indicates less association of the IW with increasing concentrations of DMSO for both the supercooled temperature and 350 K. The $g(r)$ of

the ID behaves opposite to that from 250 K to 350 K at 5 and 25%. An increase in DMSO concentration usually leads to an increase in the area per lipid bilayer as DMSO molecules intercalate between lipid heads, disrupting the packing of lipid molecules and causing them to spread apart, thus increasing the available area per lipid.

3.2.1 Population of interfacial and hydrophobic water and DMSO

As the IW and ID are continuously residing at the interface regime, they are considered bound and labeled as N_B. The ratio of N_B to N_L (N_L is the total number of lipids) for both the ID and IW are shown in Figure S7 of

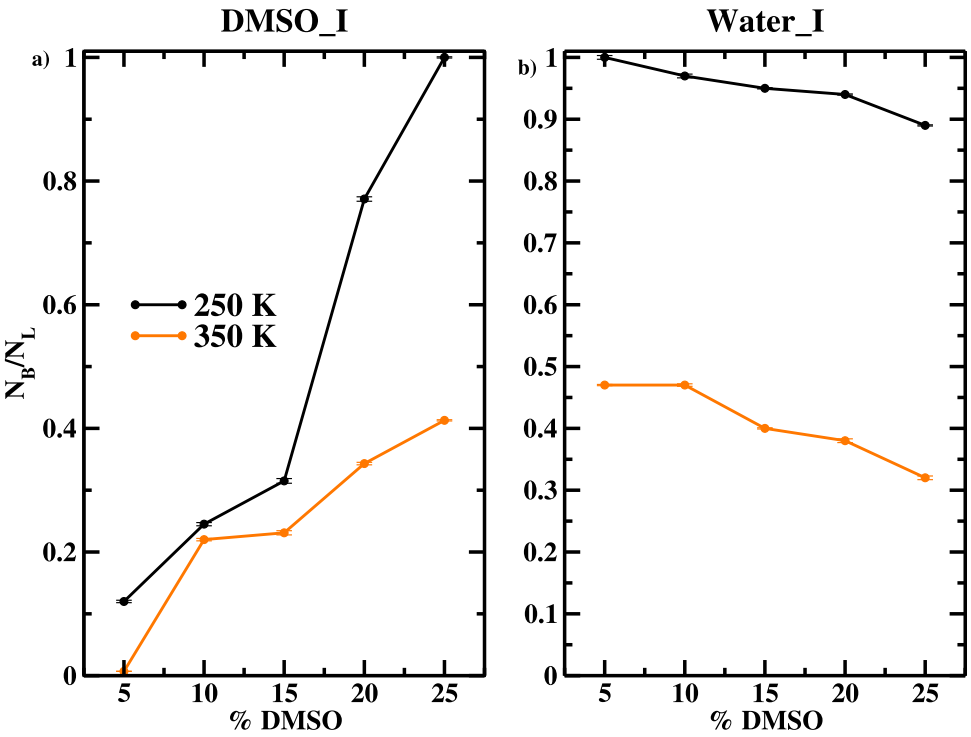

Fig. 8 Number of bound interfacial **a** DMSO and **b** water per lipid continuously residing at the interface for 50 ps shown for all the bilayers containing different concentrations of DMSO. The error bar depicts the block average over 5 sets of data

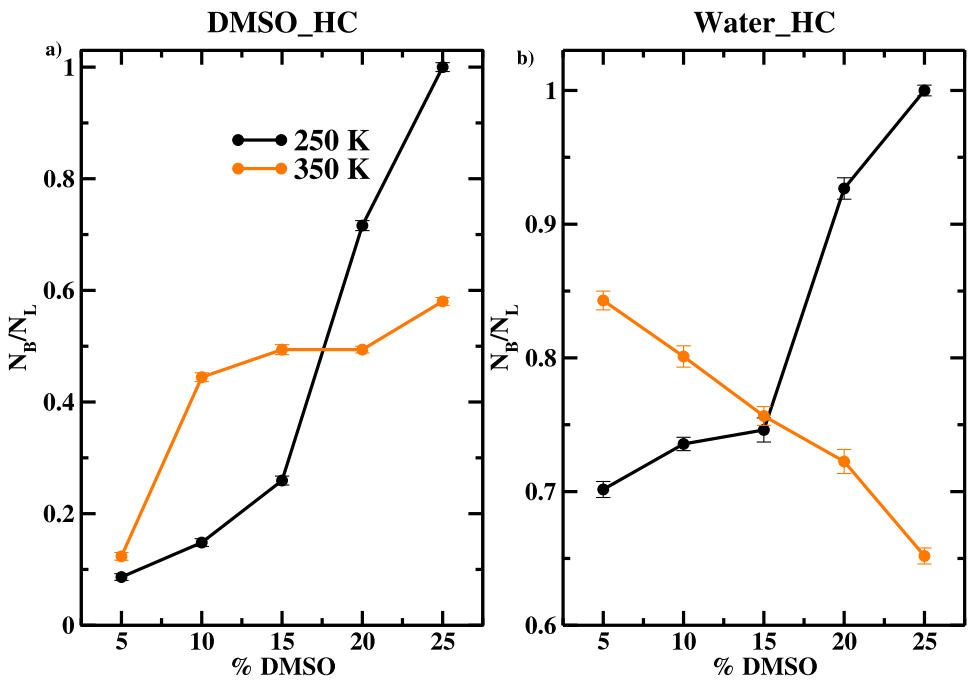

Fig. 9 Numbers of **a** DMSO and **b** water per lipid at the hydrophobic core (HC) residing for at least a single time frame of the simulation trajectory are shown for varying concentrations of DMSO for two extreme temperatures. The error bar depicts the block average over five sets of data

SI with respect to temperatures. $\frac{N_B}{N_L}$ increases with lowering the temperature for both ID and IW, demonstrating more bound DMSO and water per lipid with supercooling. In Fig. 8 where the ratio is shown for the two extreme temperatures studied, the population of bound DMSO increases with increasing concentration of DMSO for all temperatures and the population of bound water decreases with a rise in DMSO concentration. However, in Figure S7 of SI, the population of bound water decreases with increasing concentration of DMSO till 300 K while cooling. After 300 K, as the bilayer goes to the supercooled regime, the population of the bound water does not decrease for 20 and 25%. As the bound water and DMSO reside between the lipid heads, their population affects the expansion of the area per lipid. The higher number of bound water and DMSO for 20 and 25% at supercooled temperature leads to an increase in area per lipid, which shifts the gel phase to the fluid phase.

Upon comparing the population of DMSO and water in the HC for two extreme temperatures, i.e., 250 K and 350 K (Fig. 9), it is found that the population of bound DMSO increases with DMSO concentration for both temperatures. However, the increase in the population is drastically high for 20 and 25% at 250 K compared to 350 K. The population of bound water decreases with increasing concentration of DMSO at 350 K, which behaves oppositely for 250 K. At 250 K, a greater number of DMSO and water molecules are found within the HC for 20 and 25% compared to that at 350 K. This abundance of DMSO and water in the HC in combination with the increased population of ID and IW contributes to the increased fluidity of the lipid chains and heads at supercooled temperature for 20 and 25% DMSO. Conversely, at 350 K, fewer water molecules are observed within the HC, particularly with an elevated concentration of DMSO in the bilayer. Thus, the increased fluidity in the bilayer at supercooled temperature for 20 and 25% DMSO is primarily attributed to a higher number of bound DMSO and water molecules at the interface as well as those traversing the HC.

3.3 Percolation

To understand the effect of interface DMSO on the gel-to-fluid phase transition of the bilayer at supercooled temperature, a two-dimensional percolation threshold is calculated for interface DMSO and water for all cases. The percolating threshold signifies a drastic structural change from a disconnected path to a connected path of an infinite network. The infinite network emerges as the largest cluster of DMSO or water at the interface. The dimensionality of this largest cluster is characterized by the effective fractal dimension d_f. In an ideal 2D system, the percolation threshold is associated with $d_f \simeq 1.89$, while in 3D systems, it is approximately 2.53. [56] Below the percolation threshold, the components exist as an ensemble of small clusters. Conversely, above the threshold, the infinite network spans the entire system. The fractal structure of the largest cluster is evaluated from its cumulative radial distribution function, $m(r)$. $m(r)$ is fitted to the equation

$$m(r) \sim r^{d_f}. \tag{5}$$

d_f is extracted from the fitting of $m(r)$ for interfacial DMSO–DMSO and interfacial water–water. Figure 10 shows that the d_f of the IW is above the percolation threshold irrespective of the temperature and the DMSO concentration. d_f of DMSO is above the percolation threshold for 25% DMSO concentration and below the threshold for 5% DMSO concentration for all temperatures. For lower concentrations of DMSO until 15%, the d_f values are below the threshold, suggesting a very ordered homogeneous distribution of small clusters, specifically at supercooled temperature. As temperature increases, d_f of DMSO increases and shifts closer to the threshold. To get insights into the nature of phase transitions, the d_f values of DMSO and water are presented with the APLH for varying concentrations of DMSO at each temperature as shown in Fig. 10. Interestingly, the shifting of the d_f of DMSO toward the percolation threshold is accompanied by the increase in the respective APLH. The increment of APLH and achieving fluidity associated with an increase in d_f suggest that the DMSO percolation at the interface assists in shifting the gel-to-fluid phase transition of the bilayer.

3.4 Mean squared displacement of interface water and interface DMSO

To understand the dynamics of interface DMSO and water on the bilayer surface, lateral mean squared displacement (MSD_{XY}) is computed using the following equation,

$$\langle \delta r_{lat}^2(t) \rangle = \frac{1}{N} \sum_{i=1}^{N} \left\langle [r_i(t+t') - r_i(t')]^2 \right\rangle_{t'}. \tag{6}$$

Figure S8 of SI shows the lateral MSD of lipids, IW, and ID for all temperatures and all DMSO concentrations, and Fig. 11 represents the lateral MSD of lipid, IW, and ID of the bilayers with two extreme temperatures and DMSO concentrations. The MSD_{XY} increases with temperature for all cases, as seen in Figure S7 of SI. The MSD_{XY} of the lipids, IW, and ID are in the sub-diffusive regime for 100 ps. The MSD_{XY} of the lipids in the presence of 5%

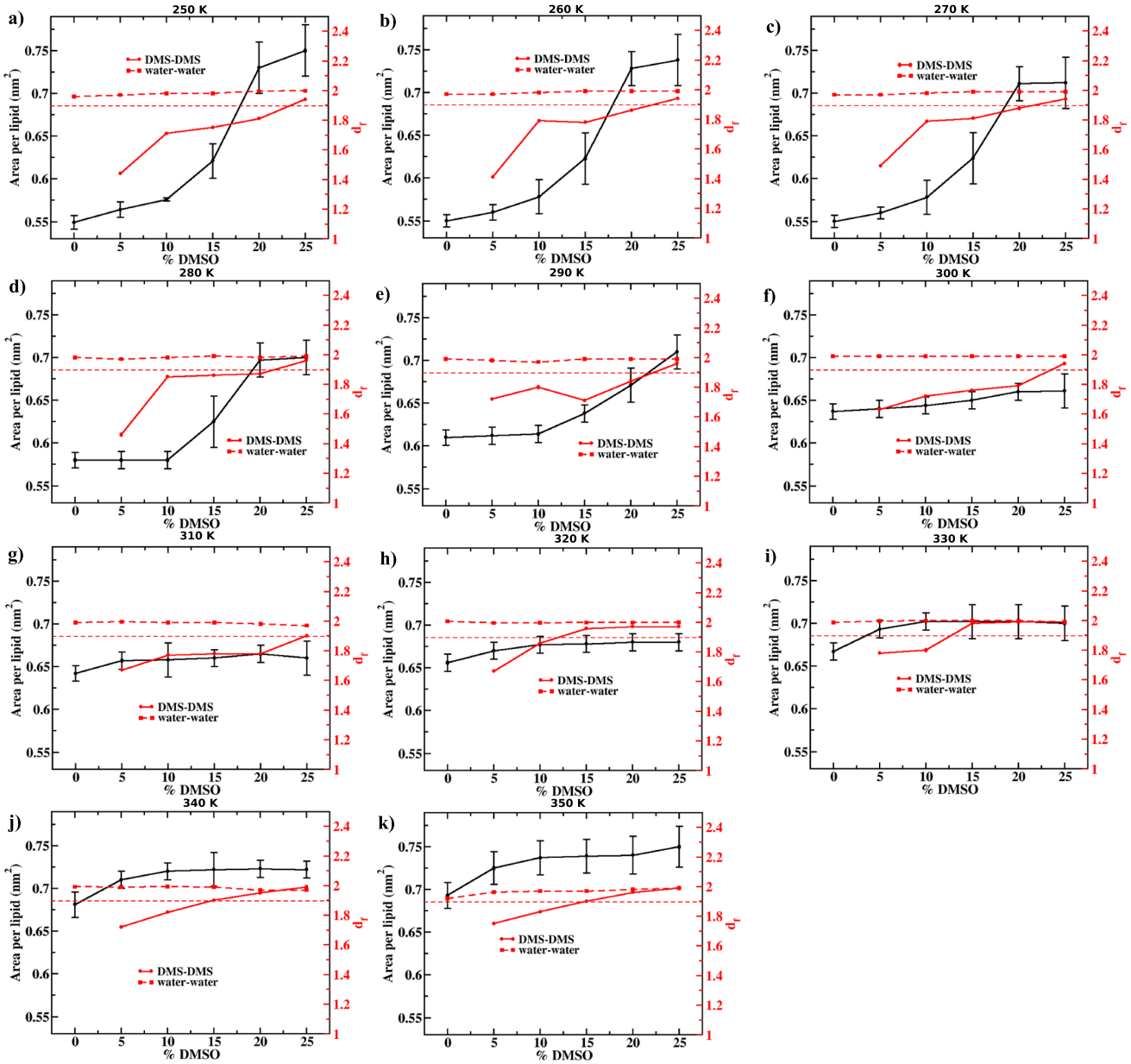

Fig. 10 Comparision of d_f and APLH of the interface DMSO and water for each of the studied temperatures. The red dashed line depicts the percolation threshold

DMSO is the lowest at 250 K, since the bilayer is at the gel phase at supercooled temperature. With increasing DMSO concentration from 5 to 25%, the MSD_{XY} of the lipids at 250 K increases, indicating enhanced fluidity of the lipids with 25% DMSO. The behaviors of IW and ID are opposite to that of the lipids. At 250 K, MSD_{XY} of the IW and ID do not differ between the 5 and 25% DMSO concentrations. The difference increases at 350 K. The addition of DMSO reduces the MSD_{XY} of the IW and ID significantly at 350 K due to the crowding effect of DMSO. Thus, the increase in bilayer fluidity at supercooled temperature due to the addition of DMSO is reflected in enhanced MSD_{XY} of lipids.

4 Conclusion

Understanding the effect of DMSO concentration on the fluidity of bilayers at the supercooled regime is crucial for a better understanding of cell banking and cryopreservation mechanisms. To this end, a total of 165.0198 μs

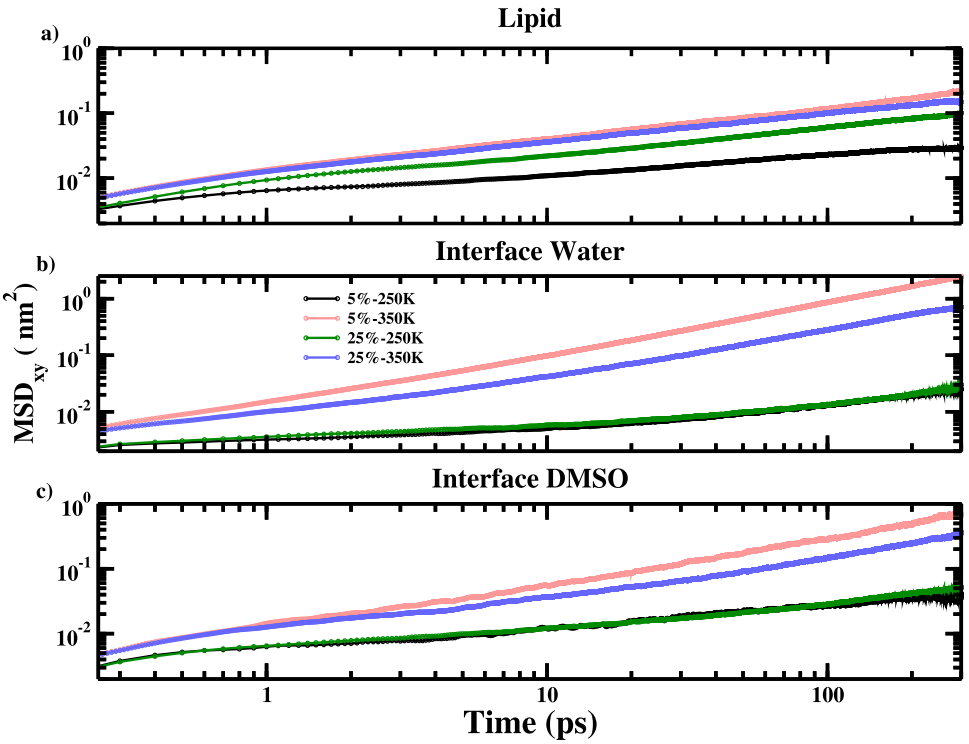

Fig. 11 Lateral MSD of **a** lipid, **b** IW, and **c** ID for two extreme temperatures and two extreme DMSO concentrations

long all-atom molecular dynamics simulations of DMPC lipid membranes are performed with a rapid cooling from 350 to 250 K. Each bilayer is equilibrated for a total simulation duration of 2 μs, followed by a production simulation of 500.3 ns. The cooling rate used in our study is several orders of magnitude faster than that used in the cryopreservation techniques [37]. With supercooling, the bilayer undergoes a fluid-to-gel phase transition in the absence of DMSO, evident from a drastic change in area per head group and chain order parameter. As DMSO concentration increases, the drastic changes reduce, and the bilayers at supercooled temperatures slowly shift from the gel to the fluid phase. For the bilayers comprising of 20% and 25%, DMSO, an anomalous contraction is observed while cooling from 300 to 280 K, which is accompanied by an increase in the area per lipid and a decrease in the order parameter. With increasing concentrations of DMSO, both DMSO and water penetrate the hydrophobic core. The penetration in the hydrophobic core becomes energetically more favorable at supercooled temperature compared to the higher temperature with an increase in DMSO concentration, specifically at 20 and 25%. Similarly, the population of bound DMSO and water at the interface and the hydrophobic core increases with DMSO concentration to a larger extent at supercooled temperature compared to that at higher temperature, e.g., 350 K. Since the DMSO and water at the interface reside between lipid heads, higher population leads to an expansion in area per lipid head which is accompanied by an increase in effective fractal dimension reaching percolation threshold for 25% for all temperatures. Subsequently, higher penetration of DMSO and water in the hydrophobic core for 20 and 25% DMSO at supercooled temperature leads to increased disorder and fluidity of the lipid chains. The increase in DMSO concentration induces higher two dimensional mean square displacements of lipids at supercooled temperature indicating enhanced fluidity of the chains. Thus our results provide a molecular mechanism of DMSO-induced fluidity of lipid membranes at supercooled temperature. The analyses will be relevant for cell banking at cryogenic temperature in the future.

Supplementary Information The online version contains supplementary material available at https://doi.org/10.1140/epjs/s11734-024-01296-y.

Acknowledgements We are thankful to the computational facility provided by the Indian Institute of Technology, Jodhpur. We thank Prof. Alexander Lyubartsev for the useful discussions on the applicability of Slipid force field on DMPC bilayers.

Author contributions

SS: data curation, formal analysis, investigation, methodology, software, writing—original draft preparation. PD: data curation, formal analysis. AD: conceptualization, funding acquisition, project administration, resources, supervision, validation, and editing.

Data availability The data that support the findings of this study are available within the article.

Code availability Not applicable.

Declarations

Conflict of interest The authors have no conflicts to disclose.

Ethics approval Not applicable.

Consent to participate Not applicable.

Consent for publication Not applicable.

References

1. K.A. Murray, M.I. Gibson, Chemical approaches to cryopreservation. Nat. Rev. Chem. **6**(8), 579–593 (2022)
2. M. Mizuno, T. Matsuzaki, N. Ozeki, H. Katano, H. Koga, T. Takebe, H.Y. Yoshikawa, I. Sekiya, Cell membrane fluidity and ros resistance define dmso tolerance of cryopreserved synovial mscs and huvecs. Stem Cell Res. Ther. **13**(1), 177 (2022)
3. T.H. Jang, S.C. Park, J.H. Yang, J.Y. Kim, J.H. Seok, U.S. Park, C.W. Choi, S.R. Lee, J. Han, Cryopreservation and its clinical applications. Integr. Med. Res. **6**(1), 12–18 (2017)
4. J. Meneghel, P. Kilbride, G.J. Morris, Cryopreservation as a key element in the successful delivery of cell-based therapies—a review. Front. Med. **7**, 592242 (2020)
5. B.P. Best, Cryoprotectant toxicity: facts, issues, and questions. Rejuv. Res. **18**(5), 422–436 (2015)
6. K.W. Yong, L. Laouar, J.A. Elliott, N.M. Jomha, Review of non-permeating cryoprotectants as supplements for vitrification of mammalian tissues. Cryobiology **96**, 1–11 (2020)
7. S. Park, D.R. Lee, J.S. Nam, C.W. Ahn, H. Kim, Fetal bovine serum-free cryopreservation methods for clinical banking of human adipose-derived stem cells. Cryobiology **81**, 65–73 (2018)
8. D.J. Kozuch, F.H. Stillinger, P.G. Debenedetti, Effects of trehalose on lipid membranes under rapid cooling using all-atom and coarse-grained molecular simulations. J. Phys. Chem. B **125**(20), 5346–5357 (2021)
9. S. Sahu, A. Garg, R. Saini, A. Debnath, Interface water assists in dimethyl sulfoxide crossing and poration in model bilayer. Langmuir **40**(11), 5764–5775 (2024)
10. S. Sahu, H. Srinivasan, S.E. Jadhav, V.K. Sharma, A. Debnath, Aspirin-induced ordering and faster dynamics of a cationic bilayer for drug encapsulation. Langmuir **39**(46), 16432–16443 (2023)
11. H.K. Shobhna, Kashyap, Deciphering ethanol-driven swelling, rupturing, aggregation, and fusion of lipid vesicles using coarse-grained molecular dynamics simulations. Langmuir **38**(8), 2445–2459 (2022)
12. G.D. Elliott, S. Wang, B.J. Fuller, Cryoprotectants: a review of the actions and applications of cryoprotective solutes that modulate cell recovery from ultra-low temperatures. Cryobiology **76**, 74–91 (2017)
13. D. Lysak, M. Brychtová, M. Leba, M. Čedíková, D. Georgiev, P. Jindra, T. Vlas, M. Holubova, Long-term cryopreservation does not affect quality of peripheral blood stem cell grafts: a comparative study of native, short-term and long-term cryopreserved haematopoietic stem cells. Cell Transpl. **30**(0963–6897), 1555–3892 (2021)
14. S.R. Panch, S.K. Srivastava, N. Elavia, A. McManus, S. Liu, P. Jin, S.L. Highfill, X. Li, P. Dagur, J.N. Kochenderfer et al., Effect of cryopreservation on autologous chimeric antigen receptor t cell characteristics. Mol. Ther. **27**(7), 1275–1285 (2019)
15. D. Moldovan, D. Pinisetty, R.V. Devireddy, Molecular dynamics simulation of pore growth in lipid bilayer membranes in the presence of edge-active agents. Appl. Phys. Lett. **91**(20), 204104 (2007)
16. Z.P. Nagy, D. Shapiro, C.C. Chang, Vitrification of the human embryo: a more efficient and safer in-vitro fertilization treatment. Fertil. Steril. **113**(2), 241–247 (2020)
17. M. Verheijen, M. Lienhard, Y. Schrooders, O. Clayton, R. Nudischer, S. Boerno, B. Timmermann, N. Selevsek, R. Schlapbach, H. Gmuender et al., Dmso induces drastic changes in human cellular processes and epigenetic landscape in vitro. Sci. Rep. **9**(1), 4641 (2019)
18. S. Adler, C. Pellizzer, M. Paparella, T. Hartung, S. Bremer, The effects of solvents on embryonic stem cell differentiation. Toxicol. In Vitro **20**(3), 265–271 (2006)

19. R. Yamaguchi, M. Takanashi, M. Ito, A. Ogawa, M. Hashimoto, Y. Ishii, T. Mazda, K. Tadokoro, K. Nakajima, M. Minami, Plasticizer concentration in cord blood cryopreserved with dmso. Bone Marrow Transpl. **49**(1), 157–158 (2014)
20. C. Morris, L. de Wreede, M. Scholten, R. Brand, A. van Biezen, A. Sureda, E. Dickmeiss, M. Trneny, J. Apperley, P. Chiusolo et al., Should the standard dimethyl sulfoxide concentration be reduced? results of a European group for blood and m arrow t ransplantation prospective noninterventional study on usage and side effects of dimethyl sulfoxide. Transfusion **54**(10), 2514–2522 (2014)
21. S. Maral, M. Albayrak, C. Pala, A. Yildiz, O. Sahin, H.B. Ozturk, Dimethyl sulfoxide-induced tonic-clonic seizure and cardiac arrest during infusion of autologous peripheral blood stem cells. Cell Tissue Bank. **19**(4), 831–832 (2018)
22. P. Westh, Preferential interaction of dimethyl sulfoxide and phosphatidyl choline membranes. Biochim. Biophys. Acta (BBA) Biomembr. **1664**(2), 217–223 (2004)
23. R. Raju, S.J. Bryant, B.L. Wilkinson, G. Bryant, The need for novel cryoprotectants and cryopreservation protocols: insights into the importance of biophysical investigation and cell permeability. Biochim. Biophys. Acta (BBA) Gen. Subj. **1865**(1), 129749 (2021)
24. S. Shobhna, M. Kumari, H.K. Kashyap, A coarse-grained model of dimethyl sulfoxide for molecular dynamics simulations with lipid membranes. J. Chem. Phys. **153**(3) (2020)
25. P. Kumari, H.K. Kashyap, Dmso induced dehydration of heterogeneous lipid bilayers and its impact on their structures. J. Chem. Phys. **151**(21) (2019)
26. P. Kumari, S. Kaur, S. Sharma, H.K. Kashyap, Impact of amphiphilic molecules on the structure and stability of homogeneous sphingomyelin bilayer: insights from atomistic simulations. J. Chem. Phys. **148**(16) (2018)
27. A.K. Sum, J.J. de Pablo, Molecular simulation study on the influence of dimethylsulfoxide on the structure of phospholipid bilayers. Biophys. J . **85**(6), 3636–3645 (2003)
28. R. Notman, M. Noro, B. O'Malley, J. Anwar, Molecular basis for dimethylsulfoxide (dmso) action on lipid membranes. J. Am. Chem. Soc. **128**(43), 13982–13983 (2006)
29. A.A. Gurtovenko, M. Patra, M. Karttunen, I. Vattulainen, Cationic dmpc/dmtap lipid bilayers: molecular dynamics study. Biophys. J . **86**(6), 3461–3472 (2004)
30. A.A. Gurtovenko, I. Vattulainen, Pore formation coupled to ion transport through lipid membranes as induced by transmembrane ionic charge imbalance: atomistic molecular dynamics study. J. Am. Chem. Soc. **127**(50), 17570–17571 (2005)
31. C.J. Malajczuk, S.S. Stachura, J.O. Hendry, R.L. Mancera, Redefining the molecular interplay between dimethyl sulfoxide, lipid bilayers, and dehydration. J. Phys. Chem. B **126**(13), 2513–2529 (2022)
32. J.P. Jambeck, A.P. Lyubartsev, Another piece of the membrane puzzle: extending slipids further. J. Chem. Theory Comput. **9**(1), 774–784 (2013)
33. F. Grote, A.P. Lyubartsev, Optimization of slipids force field parameters describing headgroups of phospholipids. J. Phys. Chem. B **124**(40), 8784–8793 (2020)
34. J.L. Abascal, C. Vega, A general purpose model for the condensed phases of water: Tip4p/2005. J. Chem. Phys. **123**(23), 234505 (2005)
35. J. Wang, R.M. Wolf, J.W. Caldwell, P.A. Kollman, D.A. Case, Development and testing of a general amber force field. J. Comput. Chem. **25**(9), 1157–1174 (2004)
36. K. Sprenger, V.W. Jaeger, J. Pfaendtner, The general amber force field (gaff) can accurately predict thermodynamic and transport properties of many ionic liquids. J. Phys. Chem. B **119**(18), 5882–5895 (2015)
37. C.J. Hunt, Cryopreservation: vitrification and controlled rate cooling. Stem Cell Bank. Concepts Protoc. **1590**, 41–77 (2017)
38. U. Essmann, L. Perera, M.L. Berkowitz, T. Darden, H. Lee, L.G. Pedersen, A smooth particle mesh ewald method. J. Chem. Phys. **103**(19), 8577–8593 (1995)
39. A. Lemak, N. Balabaev, On the berendsen thermostat. Mol. Simul. **13**(3), 177–187 (1994)
40. H.J.C. Berendsen, J.P.M. Postma, W.F. van Gunsteren, A. DiNola, J.R. Haak, Molecular dynamics with coupling to an external bath. J. Chem. Phys. **81**(8), 3684–3690 (1984)
41. G. Bussi, D. Donadio, M. Parrinello, Canonical sampling through velocity rescaling. J. Chem. Phys. **126**(1), 014101 (2007)
42. M. Parrinello, A. Rahman, Polymorphic transitions in single crystals: a new molecular dynamics method. J. Appl. Phys. **52**(12), 7182–7190 (1981)
43. @articleABRAHAM201519, GROMACS: High-performance molecular simulations through multi-level parallelism from laptops to supercomputers. SoftwareX **1–2**, 19–25 (2015)
44. S. Malik, A. Debnath, Dehydration induced dynamical heterogeneity and ordering mechanism of lipid bilayers. J. Chem. Phys. **154**(17), 174904 (2021)
45. K. Jacobson, O.G. Mouritsen, R.G. Anderson, Lipid rafts: at a crossroad between cell biology and physics. Nat. Cell Biol. **9**(1), 7–14 (2007)
46. T. Seki, S. Sun, K. Zhong, C.C. Yu, K. Machel, L.B. Dreier, E.H. Backus, M. Bonn, Y. Nagata, Unveiling heterogeneity of interfacial water through the water bending mode. J. Phys. Chem. Lett. **10**(21), 6936–6941 (2019)
47. J.H. Crowe, L.M. Crowe, Preservation of mammalian cells-learning nature's tricks. Nat. Biotechnol. **18**(2), 145–146 (2000)
48. S. Malik, S. Karmakar, A. Debnath, Relaxation time scales of interfacial water upon fluid to ripple to gel phase transitions of bilayers. J. Chem. Phys. **158**(11), 114503 (2023)

49. S. Kundu, S. Malik, M. Ghosh, S. Nandi, A. Pyne, A. Debnath, N. Sarkar, A comparative study on dmso-induced modulation of the structural and dynamical properties of model bilayer membranes. Langmuir **37**(6), 2065–2078 (2021)
50. A. Srivastava, A. Debnath, Hydration dynamics of a lipid membrane: hydrogen bond networks and lipid-lipid associations. J. Chem. Phys. **148**(9) (2018)
51. A. Srivastava, S. Malik, A. Debnath, Heterogeneity in structure and dynamics of water near bilayers using tip3p and tip4p/2005 water models. Chem. Phys. **525**, 110396 (2019)
52. A. Srivastava, S. Karmakar, A. Debnath, Quantification of spatio-temporal scales of dynamical heterogeneity of water near lipid membranes above supercooling. Soft Matter. **15**(47), 9805–9815 (2019)
53. A. Srivastava, S. Malik, S. Karmakar, A. Debnath, Dynamic coupling of a hydration layer to a fluid phospholipid membrane: intermittency and multiple time-scale relaxations. Phys. Chem. Chem. Phys. **22**(37), 21158–21168 (2020)
54. S. Malik, S. Karmakar, A. Debnath, Quantifying dynamical heterogeneity length scales of interface water across model membrane phase transitions. J. Chem. Phys. **158**(9), 091103 (2023)
55. A. Debnath, K. Ayappa, V. Kumaran, P.K. Maiti, The influence of bilayer composition on the gel to liquid crystalline transition. J. Phys. Chem. B **113**(31), 10660–10668 (2009)
56. D. Stauffer, A. Aharony, Introduction to Percolation Theory (Taylor & Francis, 2018)